Novel Multilevel STATCOM for Power System Stability Enhancement on DFIG-Based Wind Farms

R. S. Camargo, A. E. A. Amorim, E.J. Bueno, L. F. Encarnação

***Abstract*-- This work proposes the evaluation of the multilevel topology based on three-phase cells with a Single DC-link Cascaded H Bridge converter (SDC-CHB) with Model Predictive Control (MPC) as Static Synchronous Compensator (STATCOM) used to support DFIG wind farm operation. The well-known Hydro-Quebec system containing a 9 MW DFIG-based wind farm was chosen as a test bench to evaluate the proposed SDC-CHB steady and transient dynamic response to contribute to the DFIG fault ride-through. Simulation results demonstrate that the proposed topology enhances the power system stability and power quality, improving the voltage profile, on average, by 10% during symmetrical and asymmetrical faults. Furthermore, the SDC-CHB and MMC-CHB parametric study is presented proving the proposed topology robustness. Both topologies present similar steady and transient dynamic responses, corroborating that the proposed multilevel converter contributes to the DFIG fault ride-through with an enhanced topology when compared with classical multilevel converters.**

***Keywords*: Power Systems Dynamics; Integration of Renewable Energy Sources; Power Electronics; DFIG-based wind farm; STATCOM; Multilevel Converters.**

I. Introduction

THE wind energy conversion systems based on Doubly-Fed Induction Generator (DFIG) are consolidating as a relevant source on power systems around the world. This configuration is the most widely used for high-power wind turbines, above 1MW [1].

However, the direct connection between the DFIG stator and the grid may cause some issues to this system. The major problem is that DFIG-based turbines are very sensitive to grid voltage disturbances and faulty situations caused by lightning, hurricanes, or equipment tripping, for instance [2]. These sudden variations on terminal voltage create an imbalance between the machine fluxes before and during the fault. In these situations, rotor electromotive force (EMF) increases significantly, leading to overvoltage and overcurrent on the rotor circuit, which could be hazardous to the power converter [3].

Due to the major importance of wind power on the electric grid, its disconnection during fault situations may lead to instabilities and worsening of the voltage surge. For this reason, the new grid codes have established strict requirements concerning wind generator's behavior during these situations. The requirements for fault ride-thought are related to uninterrupted connection, power delivery, and contribution to the grid stability during a certain time interval, according to the fault severity [4].

There are several solutions proposed in the literature to accomplish grid code demands and at the same time ensure DFIG's reliable and safe operation [5].

Among the solutions to contribute to fault supportability and grid stability the Flexible AC Transmission Systems (FACTS), in particular Static Synchronous Compensator (STATCOM), are widely employed. The STATCOM contributes to voltage regulation at the point of common coupling (PCC) despite power generation oscillation due to wind conditions and load variations. Also, the use of STATCOM has been reported in fault conditions, the device capability to inject reactive power assists to PCC voltage reestablish and to the mitigation of the harmful effects on DFIG power converter [6]-[8].

Recent works show the application of STATCOM to enhance DFIG low voltage ride-through (LVRT) capability for symmetrical and asymmetrical faults [9] demonstrating that STATCOM can be effective to mitigate power oscillations and suppress current harmonics in DFIG-based systems [10]. The study of power systems with the presence of DFIG-based wind farms and STATCOM is well established in literature with its positive results corroborated by several current works [11],[12]. These works ensure that the STATCOM can increase the transient stability in several grid configurations during grid faults, voltage sag, and voltage swell.

Thus, different multilevel STATCOM topologies have been studied to improve the STATCOM dynamics, reliability, voltage stress, and other features. It is well established that multilevel converters have a superior steady and transient state response over conventional converters [13], [14]. Thus, several works discuss the benefits and harms of multilevel converters topologies such as the number of components, modularity, voltage DC-link control, and other features [15]. The best-known multilevel converter topologies are diode-clamped multilevel converter (DCMC) [16], capacitor-clamped multilevel converter (CCMC) [15], modular multilevel converter (MMC) [16], cascaded H bridge converter (MMC-CHB) [15], [16], mixed-level hybrid multilevel cells (MHMC) [15] and asymmetric hybrid multilevel cells (AHMC) [15].

This work was supported in part by the Fundação de Amparo à Pesquisa e Inovação do Espírito Santo (FAPES) under Grants 536/2018 and 117/2019.

R. S. Camargo is with the Department of Control and Automation Engineering, Federal Institute of Espírito Santo (IFES), 29173-087 Brazil (e-mail of the corresponding author: rscamargo@ifes.edu.br).

A. E. A. Amorim is with Federal Institute of Espírito Santo, Sao Mateus, ES 29932540 Brazil (e-mail: arthur.amorim@ifes.edu.br).

E.J. Bueno is with Department of Electronics, Universidad de Alcalá (UAH), Madrid, 28801 Spain (e-mail: emilio.bueno@uah.es).

L. F. Encarnação is with Federal University of Espírito Santo, Vitória, ES 29075910 Brazil (e-mail: lucas.encarnacao@ufes.br).

Paper submitted to the International Conference on Power Systems Transients (IPST2021) in Belo Horizonte, Brazil June 6-10, 2021.

The DCMC and CCMC have a limitation due to the use of many components for converters with three or more output voltage levels. To overcome this limitation, some authors proposed a mixed-level hybrid based on DCMC (MHMC-DCMC) and CCMC (MHMC-CCMC). However, these topologies are based on single-phase cells, which have higher DC voltage oscillation at a low-frequency range with twice the fundamental grid frequency (2ω) jeopardizing the DC-link voltage control. The same issue can be extended to the MMC and CHB topologies. Despite having an excellent ratio between the number of components and voltage levels, these converters also present problems related to the DC-link voltage control because of the single-phase power flow. Lastly, although the AHMC displays an excellent number of components, this topology does not have a modular structure and has different DC voltage values making the DC-link control more complex.

To overcome the disadvantages, aggregating only the advantages of each topology, the authors proposed a novel cascaded multilevel topology based on three-phase cells with a single DC-link cascaded H bridge converter (SDC-CHB) with a reduced number of components, modular structure, and simpler DC-link voltage control where the topology conception and preliminary results were presented in [17].

This work demonstrates the effectiveness of the novel SDC-CHB converter for STATCOM application, presented in [14], to enhance the DFIG-based wind farms stability and, concomitantly, highlighting the advantages of the proposed multilevel converter. The SDC-CHB STATCOM is evaluated in the well-known Hydro-Quebec system with a 9 MW wind farm of six 1.5 MW wind turbines connected to a 120 kV grid through a 25 kV with 30-kilometer distribution system [18]. Furthermore, SDC-CHB STATCOM behavior is compared to a similar device based on MMC-CHB topology with the same operational characteristics.

The paper is organized as follows: Section II presents the applied DFIG control and basic concepts. Section III presents the SDC-CHB topology, control strategy, and a discussion of the novel topology advantages over the classical multilevel topologies. Section IV presents the simulation results proving that the SDC-CHB improves the system stability and, concomitantly, highlighting the advantages of the proposed multilevel converter. Lastly, Section V presents the paper's conclusion.

II. MODELLING OF DFIG-BASED WIND FARM

This work considers a DFIG-based wind farm according to [18]. This farm consists of six 1.5 MW DFIG-based wind energy conversion systems formed by the wind turbine with pitch control, the gearbox, the wound rotor induction generator, the back-to-back power converter, and the passive filters.

A. Power converter control

The DFIG technology enables the operation in variable speed to extract maximum power from the wind using a partial converter, around 30% of DFIG rated power. The stator winding is directly connected to the grid, while the back-to-back converter feeds the rotor winding. This converter consists of two PWM Voltage Source Converters (VSC) connected through a DC-link, forming a bidirectional AC/DC/AC converter. The 60 Hz grid connects to the Grid Side Converter (GSC), which controls the DC-link voltage and the reactive power flow between the grid and the converter. The Rotor Side Converter (RSC) provides the currents to the rotor circuit according to the wind speed to ensure maximum power extraction. This converter can control stator active and reactive power independently ensuring unity power factor both in the sub and in the super synchronous operation.

The GSC references are the predetermined DC-link voltage and null reactive power. Using a cascade control loop, the output voltage, and thus the converter PWM signals are determined. The RSC control works similarly, also using cascade control loops. The stator active power reference is set according to measured wind speed and turbine model, while the reactive power reference is adjusted to zero to achieve unity power factor. These power references determine the PWM signals for the RSC.

B. Behavior during faults

To understand DFIG behavior during transients, specifically for the study of voltages dips, the modeling proposed by [3] is used. Based on the machine model, the rotor voltage is given as a function of rotor flux:

$$\vec{v}_r^r = R_r\vec{i}_r^r + \frac{d\vec{\psi}_r^r}{dt} \quad (1)$$

where $\vec{v}_r^r$ is the rotor voltage, R_r is the rotor resistance, $\vec{i}_r^r$ is the rotor current, and $\vec{\psi}_r^r$ is the rotor flux.

However, the rotor flux is the result of stator flux and rotor current interaction:

$$\vec{\psi}_r^r = \frac{L_m}{L_s}\vec{\psi}_s^r + \sigma L_r\vec{i}_r^r \quad (2)$$

where $\vec{\psi}_r^r$ is rotor flux, L_m, $L_r$and L_s are inductances, and $\sigma = 1 - L_m^2/(L_s.L_r)$. The superscript r indicates variables are referred to the rotor.

By substituting equation (2) in equation (1):

$$\vec{v}_r^r = \frac{L_m}{L_s}\frac{d}{dt}\vec{\psi}_s^r + R_r\vec{i}_r^r + \sigma L_r\frac{d}{dt}\vec{i}_r^r \quad (3)$$

The first term of this equation relates to rotor EMF and the other terms represent the voltage drop on rotor resistance and inductance due to rotor current. This equation shows that the rotor voltage is dependent on stator flux. Therefore, a variation on this flux due to voltage dips will produce overvoltage on the machine rotor, since:

$$\frac{d}{dt}\vec{\psi}_s^s = \vec{v}_s^s - R_s\vec{i}_s^s \quad (4)$$

where $\vec{v}_s^s$ is the stator voltage and R_s is the stator resistance. The superscript s indicates variables are referred to the stator.

In [19] its demonstrated that the rotor voltage can reach values far beyond converter capacity in fault situations due to the high induced EMF. Hence, if no countermeasure is taken, high currents circulate on the rotor circuit and may cause damage to the power converter switches.

To avoid converter harm, as soon as the fault is detected, some actions are taken by DFIG control. The first action is to set the RSC power reference to zero, to disable the switches,

[20]. Besides that, some protection device is activated to mitigate or diverge rotor currents [19] or also to minimize the voltage drop seen on PCC [7], [11]. In addition to this, many grid codes demand reactive power injection during the voltage sag. To comply with the requirement a STATCOM can be employed to produce the reactive power demanded by grid codes and support PCC voltage.

III. SDC-CHB and Multilevel Topologies' Comparison

The five-level SDC-CHB topology, presented in Fig. 1, is composed of six H bridge structures, two for each phase, with a single DC-link per module in a cascaded connection. Thus, the three-phase structure provides a $2/3$ reduction in the number of capacitors used compared to single-phase structures, such as the classical CHB. Besides, three-phase structures require less capacitance to provide adequate ripple values in capacitor voltages compared with single-phase structures. The reduction in the capacitance can achieve values ten times lower, as presented by equations (5) and (6), contributing to the reduction of construction costs [21], [22].

$$C_{1\theta} = \frac{P}{\omega . U_{DC} . \Delta_V} \tag{5}$$

$$C_{3\theta} = \left(\frac{1}{10}\right) \frac{P}{\omega . U_{DC} . \Delta_V} \tag{6}$$

where P is the converter active power, ω is the grid frequency, U_{DC} is the DC-link voltage, Δ_V is the DC-link voltage ripple, $C_{1\theta}$ and $C_{3\theta}$ are the capacitance of single-phase and three-phase converters, respectively.

Another advantage of the SDC-CHB topology is a lower number of components by output voltage levels ratio. As presented in Fig. 2, the SDC-CHB compared with other multilevel topologies, has the lowest number of components to achieve the same voltage levels without losing the modularity structure.

Lastly, the proposed topology is based on a full-bridge converter ensuring a unitary ratio between the single-phase peak voltage and the DC-link voltage. Most converters, except CHB, consist of a half-bridge converter, maintaining only a 50% ratio between the output voltage and the DC-link voltage. Table I summarizes the comparison of the multilevel converters.

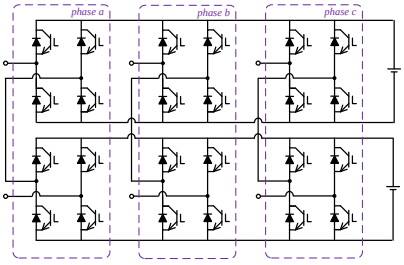

Fig. 1. CHB-SDC topology

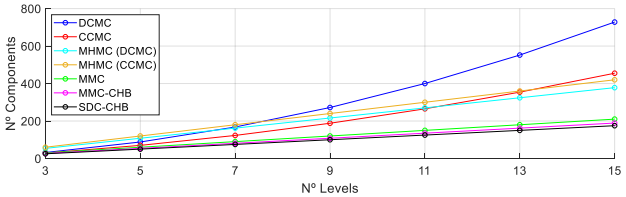

Fig. 2. Number of components by output voltage levels ratio

TABLE I
Multilevel Topologies Comparison

	DCMC	CCMC	MHMC-DCMC	MHMC-CCMC	MMC	CHB	SDC-CHB
Number of Components	*VH*	*H*	*H*	*H*	*L*	*L*	*VL*
Modularity	*N*	*N*	*Y*	*Y*	*Y*	*Y*	*Y*
2ω DC-Link oscillation	*N*	*N*	*Y*	*Y*	*Y*	*Y*	*N*
Full-Bridge	*N*	*N*	*N*	*N*	*N*	*Y*	*Y*

where *VH*, *H*, *L*, *VL*, *N*, and *Y* means very high, high, low, very low, no, and yes, respectively.

Despite the several advantages inherent to the SDC-CHB topology, this structure presents problems when a PWM strategy is applied, causing severe short circuits in its capacitors depending on the state of each semiconductor. Thus, some kind of insulation stage, for example, coupling transformers, between its modules is necessary, which would result in a substantial increase in costs.

Thus, to solve this problem without insulation stages, the SDC-CHB switching states were carried out and analyzed. Since each of the 24 semiconductor switches has only two states (ON and OFF), a five-level CHB-SDC has 2^{24} different possible combinations, that is, $16{,}777{,}216$ different switching states. However, these combinations are reduced to 2^{12} (4096) because each leg of the converter has interlocking signals, known as unipolar modulation. Studies carried out with graph theory found that only 640 of the 4096 switching states do not have internal short circuits, which corresponds to 16% of possible states. After analyzing the permissible switching states, it was observed that it would be possible to synthesize all five voltage levels of the converter with only 640 states, making its implementation possible as long as each position of the semiconductor was observed and controlled individually [23]. This characteristic is essential to produce a three-phase sine wave with low total harmonic distortion (THD) required for a STATCOM application.

Thus, instead of applying a conventional current loop with a PWM switching strategy, which would inevitably generate internal short circuits in the proposed multilevel converter, a model predictive control (MPC) is applied to the SDC-CHB. The MPC is capable of synthesizing the calculated currents by the STATCOM controller and, at the same time, avoid the prohibitive states of the SDC-CHB.

Fig. 3 presents an overview of the Hydro-Quebec system [18], used as a test bench scenario, with the proposed SDC-CHB STATCOM with the MPC. The Hydro-Quebec system, highlighted in blue, contains a 9 MW wind farm of six 1.5 MW wind turbines (DFIG wind turbine subsystem) with the DFIG controller discussed in Section II. The DFIG wind turbine system is connected to a 120 kV grid bus with a 2500MVA short circuit characteristic (SCC) with a 3:1 zero to positive ratio $(X_0/X_1 = 3)$ through a 25 kV distribution system with a 30 km length (distribution subsystem). T_{grid} and $T_{DFIG1\text{-}6}$ are grid and DFIG transformers, while T_{ground} is the zig-zag grounding transformer. The SDC-CHB MPC STATCOM, highlighted in green, is composed of two three-phase single DC-link H bridge

modules connected in the DFIG wind turbine subsystem bus through a three-phase transformer (T_{STAT}) with an open wind configuration on the secondary side.

Fig. 4 shows an overview of the model predictive control and power circuit of the SDC-CHB STATCOM, where e_{Sn} and i_{Sn} are the voltages and currents at the point of common coupling (PCC), U_{DCx} and U_{DC}^{*} are the SDC-CHB DC-link voltages, and DC-link reference voltage, U_{Sn} are the output STATCOM voltages, r, and l are the resistance and inductance filter, and l_d is the damping inductance, $Q^{*}(k+2)$ is the reference reactive power, $P_{Loss}^{*}(k+2)$ is the reference active power calculated by the MPC to regulate the DC-link capacitor voltages [24], k is the measured value and $k+2$ is the predicted state after two time steps (T_s) to compensate for the processing delay signals which have values close to one T_s, N is the total prediction states, S_{opt} is the optimal switching state, n is the phase index (a,b,c) and x is the module index (*1*,*2*). The SDC-CHB STATCOM parameters are presented in Table II.

Firstly, an outer loop control (STATCOM controller) calculates dynamically the reference reactive power in steady-state and in transient conditions to maintain the PCC voltage on 1.0 pu. During faults, the reactive injection is limited to STATCOM's current capacity. Then, the calculated reference reactive power, the measured DC-link voltages, and the measured voltages and currents at PCC are used in the MPC.

The SDC-CHB STATCOM is demonstrated as follows. Assuming that the capacitor voltages C_{DC1} and C_{DC2} are regulated (U_{DC}), the converter can synthesize five voltage levels $U_{Sn}^{N} = [-2U_{DC,} - U_{DC}, 0, +U_{DC}, +2U_{DC}]$. Thus, the predicted current $i_{Sn}(k+1)$, obtained by Kirchhoff voltage law and Euler numerical integration, is defined in equation (7).

$$i_{Sn}^{N}(k+1) = \frac{T_s}{2l+l_d}\left(e_{Sn}(k) + i_{Sn}(k)\left(\frac{2l}{T_s}+\frac{l_d}{T_s}-2r\right) - U_n^{N}(k)\right) \quad (7)$$

The predicted voltage (U_{Sn}) is calculated by the measured DC-link voltages (U_{DCx}) and the switching function $S_{nx}(k)$, which represents each module's possible switching states $S_{nx}(k) = [-1, 0, +1]$, as defined in equation (8).

$$U_n^{N}(k) = S_{n1}(k)\cdot U_{DC1}(k) + S_{n2}(k)\cdot U_{DC2}(k) \quad (8)$$

The predictive capacitor voltages $U_{DCx}(k+1)$ is calculated by the measured currents (i_{Sn}) and the switching states function $S_{nx}(k)$.

$$U_{DCx}^{N}(k+1) = U_{DCx}(k) + \frac{T_s}{C_{DCx}}\left(S_{ax}i_{Sa}(k) + S_{bx}i_{Sb}(k) + S_{cx}i_{Sc}(k)\right) \quad (9)$$

where C_{DCx} are the DC-link capacitor voltage modules.

To compensate for the processing delay signals, it is not enough to predict variables for just one time step, thus requiring the calculation of references for two time steps, that is, $(k+2)^{th}$ predicted values. The results for $(k+1)^{th}$, obtained by (7) to (9), are applied in (10) to (14). The cost function is calculated only in the $(k+2)^{th}$ instant.

$$i_{Sn}^{N}(k+2) = \frac{T_s}{2l+l_d}\left(e_{Sn} + i_{Sn}(k+1)\left(\frac{2l+l_d}{T_s}-2r\right) - U_n^{N}(k+1)\right) \quad (10)$$

$$U_n^{N}(k+1) = S_{n1}(k+1)U_{DC1}(k+1) + S_{n2}(k+1)U_{DC2}(k+1) \quad (11)$$

$$U_{DCx}^{N}(k+2) = U_{DCx}(k+1) + \frac{T_s}{C}\left(\sum_{n}^{a,b,c} S_{nx}i_{Sn}(k+1)\right) \quad (12)$$

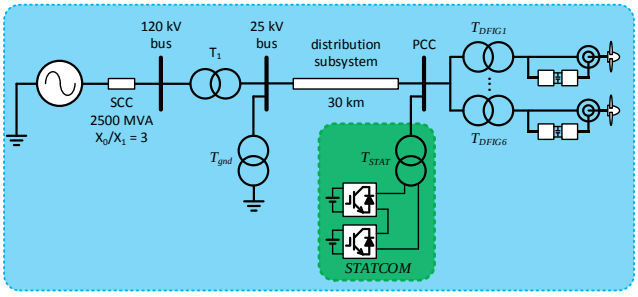

Fig. 3. Hydro-Quebec system with the proposed SDC-CHB MPC STATCOM overview

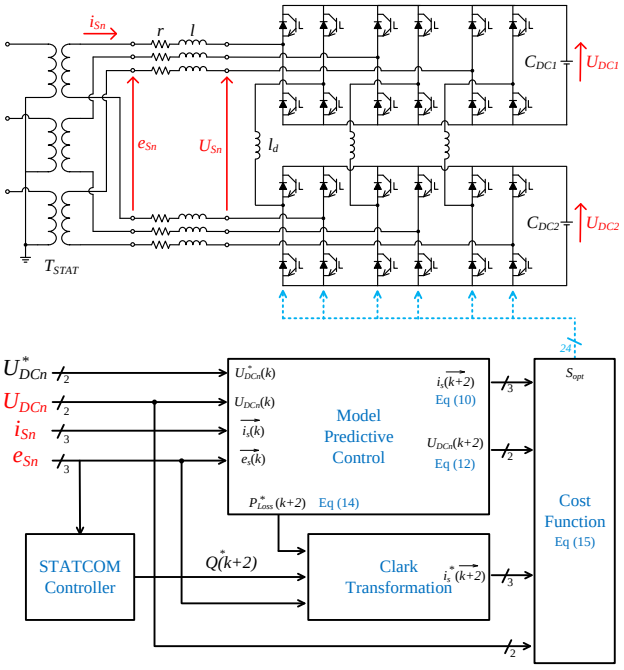

Fig. 4. MPC STATCOM CHB-SDC control overview.

TABLE II
SDC-CHB STATCOM PARAMETERS

PARAMETERS	SYMBOL	VALUE
NOMINAL POWER	(S_{STAT})	1 MVA
NOMINAL VOLTAGE	(V_{STAT})	575 V
FILTER INDUCTANCE	(L)	100 µH
FILTER RESISTANCE	(R)	25 µΩ
DC-LINK VOLTAGES	(U_{DC})	500 V
DC-LINK CAPACITANCES	(C_{DC})	30 MF
MPC TIME STEP	(T_s)	50 µS

To regulate the SDC-CHB DC-link voltages, the active predictive powers $p_{DCx}(k+2)$ are calculated to each capacitor, as presented in equation (13). Then, the total switching losses can be defined, as presented in equation (14).

$$p_{DCx}(k+2) = \frac{C}{T_s}\left[(U_{DCx}^{*}(k+2))^2 - (U_{DCx}(k+1))^2\right] \quad (13)$$

$$P_{Loss}^{*}(k+2) = \sum_{x=1}^{2} p_{DCx}(k+2) \quad (14)$$

Thus, the reference currents $i_{sn}^{*}(k+2)$ is calculated using the active $P_{Loss}^{*}(k+2)$ and reactive $Q^{*}(k+2)$ references by a Clark transformation.

Finally, the MPC cost function scan all possible switching combinations and choose which state has the smallest error between the reference and predicted signals. However, since the prohibitive states mapped by the graph theory must be avoided, a penalty is added in the cost function. The cost function

adopted in this work is shown on (15), where g^N is the cost for all the switching states, W_i and W_{UDC} are the weight factors and P_{en} is the described penalty.

$$g^N = W_i\left[\sum_{n}^{a,b,c}\left(i_{sn}^{*}(k+2) - i_{sn}^{N}(k+2)\right)^2\right] + W_{UDC}\left[\sum_{x}^{1,2}\left(U_{DCx}^{*}(k+2) - U_{DCx}^{N}(k+2)\right)^2\right] + P_{en} \quad (15)$$

IV. Simulation Results

The proposed SDC-CHB MPC STATCOM is evaluated in the Hydro-Quebec wind farm system using Simulink Matlab environment. The system is simulated for 10 seconds, where the first 8 seconds are used to the wind turbine electromechanical model reaches the steady-state condition. At 8.25 s the positive-sequence 120 kV bus voltage suddenly drops to 0.5 p.u for 200 ms, causing a voltage dip in the PCC. To evaluate the SDC-CHB MPC STATCOM power system enhancement, two scenarios are simulated, with and without the STATCOM.

Fig. 5 presents the rotor currents during the LVRT event. As expected, the DFIG control countermeasures, discussed in Section II, takes action limiting the rotor currents up to 1.3 pu, without and with the SDC-CHB STATCOM, proving that the STATCOM does not interfere with DFIG control. A similar analysis can be inferred in Fig. 6, where the STATCOM does not interfere with DFIG power flow.

Fig. 7 (a) presents the SDC-CHB STATCOM instantaneous active and reactive power and Fig. 7 (b) presents PCC voltage and the STATCOM current. In a steady-state, the STATCOM injects an inductive 1.0 MVAr reactive power to regulate the PCC voltage to 1.0 pu, improving the power system quality. In the transient state, during the LVRT, the STATCOM injects a capacitive 1.0 MVAr, limited to STATCOM current capacity, to enhance the grid stability, as required by the grid codes.

Fig. 8 presents the voltage profile in the steady and transient state without and with SDC-CHB and MMC-CHB STATCOM. In both STATCOM scenarios, the voltage profile is increased from 0.52 to 0.57pu, an improvement of 9.6%, proving that the proposed SDC-CHB STATCOM contribution to the system stability is similar to the MMC-CHB STATCOM.

Fig. 9 shows the SDC-CHB and MMC-CHB DC-link voltages. It's important to highlight that the same individual capacitance was used in both topologies ($C_{DC} = 30mF$). So, due to the single-phase topology, the MMC-CHB has a total capacitance three times higher ($6x30mF = 180mF$) than the SDC-CHB structure ($2x30mF = 60mF$). As presented in Fig. 9(a), the MPC is capable of dynamically regulate the DC-link voltages at 500 V without the low-frequency oscillation (2ω), even during the LVRT. In contrast, even with higher total capacitance, the MMC-CHB DC-link voltages present a greater DC-link voltage oscillation compared to SDC-CHB.

The SDC-CHB modules and total output voltage are presented in Fig. 10. As expected, each module voltage presents a three-level output voltage, Fig. 10 (a) and (b), while the total output voltage presents a five-level voltage, Fig. 10 (c), proving that even with only 16% possible states all the levels can be synthesized.

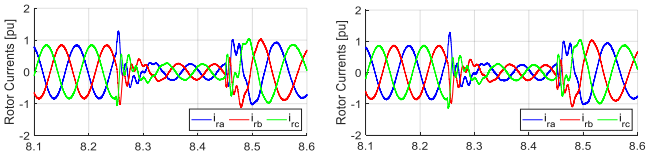

(a) (b)

Fig. 5. Rotor currents (a) without and (b) with SDC-CHB STATCOM.

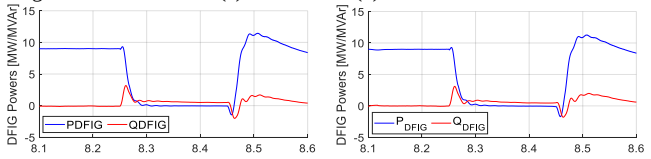

(a) (b)

Fig. 6. DFIG powers (a) without and (b) with SDC-CHB STATCOM.

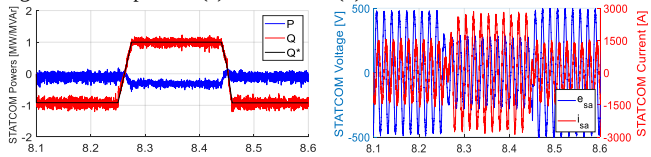

(a) (b)

Fig. 7. SDC-CHB STATCOM (a) instantaneous powers and (b) voltage/current.

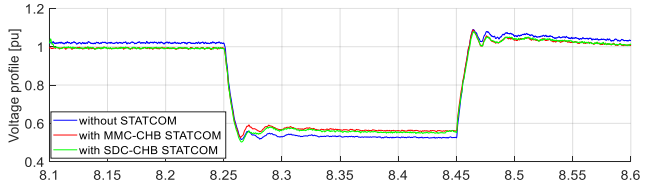

Fig. 8. Voltage profile without and with SDC-CHB and MMC-CHB STATCOM.

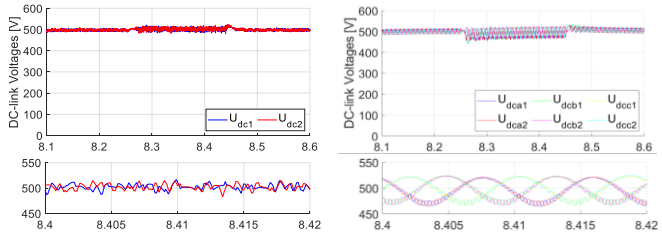

(a) (b)

Fig. 9. DC-link voltages (a) with SDC-CHB and (b) MMC-CHB.

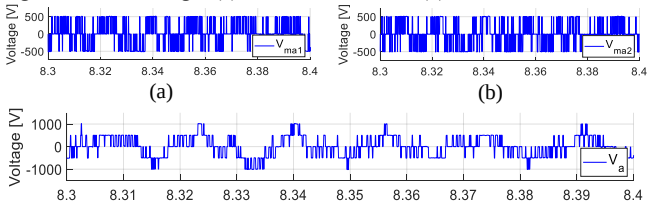

(a) (b)

(c)

Fig. 10. Upper (a) and lower (a) and total (c) SDC-CHB output voltages.

Table III presents a parametric comparison between the STATCOM based on SDC-CHB and MMC-CHB topologies. The original system benchmark has a 15m/s wind speed, 2500MVA SCC with a symmetrical fault with 50% voltage sag (SC1). Thus, several simulation scenarios were presented using both STATCOM topologies, as follows: symmetrical fault with 80% voltage sag (SC2); asymmetrical fault with 50% voltage sag (SC3); asymmetrical fault with 80% voltage sag (SC4); 1250 MVA SCC (SC5), and 10m/s wind speed (SC6). Table III presents the voltage profile at PCC (p.u.) and the percentual contribution during LVRT for each scenario. The simulation results show that the SDC-CHB has similar behavior with the classical MMC-CHB structure.

TABLE III
PARAMETRIC COMPARISON – VOLTAGE BUS (P.U.)

SC	WITHOUT STATCOM	SDC-CHB STATCOM $C_{DCx} = 30mF$ $\sum C_{DCx} = 60mF$	MMC-CHB STATCOM $C_{DCnx} = 30mF$ $\sum C_{DCnx} = 180mF$
1	0.52	0.57 (9.6%)	0.57 (9.6%)
2	0.25	0.28 (12%)	0.28 (12%)
3	0.82	0.90 (9.8%)	0.90 (9.8%)
4	0.72	0.81 (12.5%)	0.81 (12.5%)
5	0.53	0.58 (9.4%)	0.57 (7.5%)
6	0.53	0.58 (9.4%)	0.57 (7.5%)

V. CONCLUSION

This work proposes a novel STATCOM multilevel converter capable to enhance the power system stability and power quality. Furthermore, the proposed topology presents several advantages when compared with classical multilevel converters. The major advantages are the lower number of components and lower capacitance values, simpler voltage DC-link control with lower DC-link voltages without losing the modularity. The short circuit stages are avoided by the developed MPC. The SDC-CHB STATCOM, which has only 1/9 of the wind farm rated power, increases the voltage profile on average, by 10% without interference with the DFIG control.

The proposed SDC-CHB topology applied to STATCOM presented satisfactory and consistent performance, compared with devices based on classical structures, such as MMC-CHB, showing similar behaviors. It stands out according to (5) and (6) that the total capacitance used in the SDC-CHB, consisting of two 30mF capacitors, is 3 times smaller than the total capacitance used in the MMC-CHB, composed of six 30mF capacitors, presenting, thus, significant constructive advantage, demonstrating the applicability of this topology and enabling the study and development of new devices based on power semiconductors.

VI. REFERENCES

[1] J. Lopez, E. Gubia, E. Olea, J. Ruiz, and L. Marroyo, "Ride Through of Wind Turbines With Doubly Fed Induction Generator Under Symmetrical Voltage Dips," in IEEE Transactions on Industrial Electronics, vol. 56, no. 10, pp. 4246-4254, Oct. 2009, doi: 10.1109/TIE.2009.2028447.

[2] D. Zhou and F. Blaabjerg, "Optimized Demagnetizing Control of DFIG Power Converter for Reduced Thermal Stress During Symmetrical Grid Fault," in IEEE Transactions on Power Electronics, vol. 33, no. 12, pp. 10326-10340, Dec. 2018, doi: 10.1109/TPEL.2018.2803125.

[3] J. Lopez, P. Sanchis, X. Roboam, and L. Marroyo, "Dynamic Behavior of the Doubly Fed Induction Generator During Three-Phase Voltage Dips," in IEEE Transactions on Energy Conversion, vol. 22, no. 3, pp. 709-717, Sept. 2007, doi: 10.1109/TEC.2006.878241.

[4] M. Baa Wafaa and L. Dessaint, "Approach to dynamic voltage stability analysis for DFIG wind parks integration," in IET Renewable Power Generation, vol. 12, no. 2, pp. 190-197, 5 2 2018, doi: 10.1049/iet-rpg.2016.0482.

[5] S. Tohidi and M. Behnam, "A comprehensive review of low voltage ride-through of doubly-fed induction wind generators," in Renewable And Sustainable Energy Reviews, vol. 57, pp. 412-419, 2016, doi: 10.1016/j.rser.2015.12.155.

[6] L. Wang and D. Truong, "Stability Enhancement of DFIG-Based Offshore Wind Farm Fed to a Multi-Machine System Using a STATCOM," in IEEE Transactions on Power Systems, vol. 28, no. 3, pp. 2882-2889, Aug. 2013, doi: 10.1109/TPWRS.2013.2248173.

[7] W. Qiao, G. K. Venayagamoorthy and R. G. Harley, "Real-Time Implementation of a STATCOM on a Wind Farm Equipped With Doubly Fed Induction Generators," in IEEE Transactions on Industry Applications, vol. 45, no. 1, pp. 98-107, Jan.-Feb. 2009, doi: 10.1109/TIA.2008.2009377.

[8] B. Pokharel and Wenzhong Gao, "Mitigation of disturbances in DFIG-based wind farm connected to weak distribution system using STATCOM," North American Power Symposium 2010, Arlington, TX, 2010, pp. 1-7, doi: 10.1109/NAPS.2010.5619587.

[9] M. K. Döşoğlu, A. Basa Arsoy, and U. Güvenç. Application of STATCOM-supercapacitor for low-voltage ride-through capability in DFIG-based wind farm. Neural Comput & Applic, vol. 28, pp. 2665–2674, 2017, doi: 10.1007/s00521-016-2219-6.

[10] K. D.E. Kerrouche, L. Wang, A. Mezouar, et al. Fractional-Order Sliding Mode Control for D-STATCOM Connected Wind Farm Based DFIG Under Voltage Unbalanced. Arab J Sci Eng 44, 2265–2280, 2019., doi: 10.1007/s13369-018-3412-y

[11] Y. K. Gounder, D. Nanjundappan and V. Boominathan, "Enhancement of transient stability of distribution system with SCIG and DFIG based wind farms using STATCOM," in IET Renewable Power Generation, vol. 10, no. 8, pp. 1171-1180, 9 2016, doi: 10.1049/iet-rpg.2016.0022.

[12] V. Kumar, A. Shukla and A. S. Pandey, "Transient Stability Enhancement of Grid Integrated DFIG Based Wind Energy Conversion System," 2020 International Conference on Contemporary Computing and Applications (IC3A), Lucknow, India, 2020, pp. 292-297, doi: 10.1109/IC3A48958.2020.233316.

[13] Camargo, R.S.; Nunes, W.T.; Dallapicula, D.M.; Encarnacao, L.F.; Simonetti, D.S.L. Design and Analysis Methodology for Modular Multilevel Converters (MMC). IEEE Lat. Am. Trans. 2018, 16, 1105–1112.

[14] Camargo, R.S.; Mayor, S.D.; Fernandes, L.D.M.; Miguel, A.M.; Bueno, E.J.; Encarnação, L.F. A Novel Cascaded Multilevel Converter Topology Based on Three-Phase Cells with Model Predictive Control. In Proceedings of the 29th IEEE International Symposium on Industrial Electronics, Delft, The Netherlands, 17–19 June 2020.

[15] Rodriguez, J.-S.; Lai, F.; Zheng, P. Multilevel inverters: A survey of topologies, controls, and applications. IEEE Trans. Ind. Electron. 2002, 49, 724–738.

[16] Zhang, G.; Li, Z.; Zhang, B.; Halang, A.W. Power Electronic Converters: Past, Present, and Future. Renew. Sustain. Energy Rev. 2018, 81, 2028–2044.

[17] Camargo, R. S.; Mayor, D. S.; Miguel, A. M.; Bueno, E. J.; Encarnação, L. F. A Novel Cascaded Multilevel Converter Topology Based on Three-Phase Cells - CHB-SDC. Energies, 13(18), 4789.

[18] Hydro-Quebec, "SimPowerSystemsTM 5 User's Guide," October 2008, (online) available: www.mathworks.com

[19] Oliveira F, Amorim A, Encarnação L, et al. Enhancing LVRT of DFIG by Using a Superconducting Current Limiter on Rotor Circuit. Energies. 2015;9(1):16. doi:10.3390/en9010016.

[20] Amorim, A. E., Carletti, D., Fardin, J. F., Encarnação, L. F., & Simonetti, D. S. (2020). A new hybrid multilevel converter for DFIG-based wind turbines fault ride-through and transient stability enhancement. Electrical Engineering, 1-16.

[21] Miranbeigi, M.; Iman-Eini, H.; Asoodar, M. A new switching strategy for transformer-less back-to-back cascaded H-bridge multilevel converter. IET Power Electron. 2014, 7, 1868–1877

[22] Davari, P.; Zare, F.; Abdelhakim, A. Active Rectifiers, and Their Control. In Control of Power Electronic Converters and Systems; Elsevier: London, UK, 2018; Volume 2.

[23] V. M. R. de Oliveira, R. S. Camargo, and L. F. Encarnação, "Field Oriented Predictive Current Control on NPC Driving an Induction Motor," 2020 IEEE International Conference on Industrial Technology (ICIT), Buenos Aires, Argentina, 2020, pp. 169-174, doi: 10.1109/ICIT45562.2020.9067236.

[24] Tarisciotti, L.; Burgos, C.; Garcia, C.; Rodriguez, J. Finite Control Set Model Predictive Control of parallel three-phase active rectifiers. In Proceedings of the 2020 IEEE International Conference on Industrial Technology (ICIT), Buenos Aires, Argentina, 26–28 February 2020.